Available online at www.sciencedirect.com
SCIENCE DIRECT®
C. R. Mecanique 333 (2005) 746–753
COMPTES RENDUS MECANIQUE
http://france.elsevier.com/direct/CRAS2B/

Shear-layer acoustic radiation in an excited subsonic jet: experimental study

Vincent Fleury, Christophe Bailly *, Daniel Juvé

Laboratoire de mécanique des fluides et d'acoustique, UMR CNRS 5509 & École centrale de Lyon, 36 avenue Guy de Collongue, 69134 Ecully cedex, France

Received 28 July 2005; accepted 30 August 2005

Presented by Geneviève Comte-Bellot

Abstract

The subharmonic acoustic radiation of a tone excited subsonic jet shear-layer has been investigated experimentally. Two jet velocities $U_j = 20$ m·s^{-1} and $U_j = 40$ m·s^{-1} were studied. For $U_j = 20$ m·s^{-1}, the natural boundary-layer at the nozzle exit is laminar. When the perturbation is applied, the fluctuations of the first and the second subharmonics of the excitation frequency are detected in the shear-layer. In addition, the first subharmonic near pressure field along the spreading jet is constituted of two strong maxima of sinusoidal shape. The far-field directivity pattern displays two lobes separated by an extinction angle $\theta^\star$ at around 85° from the jet axis. These observations follow the results of Bridges about the vortex pairing noise. On the other hand, for $U_j = 40$ m·s^{-1}, the initial boundary-layer is transitional and only the first subharmonic is observed in the presence of the excitation. The near pressure field is of Gaussian shape in the jet periphery and the acoustic far-field is superdirective as observed by Laufer and Yen. The state of the initial shear-layer seems to be the key feature to distinguish these two different radiation patterns. ***To cite this article: V. Fleury et al., C. R. Mecanique 333 (2005).***

Résumé

Rayonnement acoustique de la couche de cisaillement d'un jet subsonique excité : étude expérimentale. Le rayonnement acoustique sous-harmonique de la couche de cisaillement d'un jet subsonique excité tonalement a été étudié pour deux vitesses de jet, $U_j = 20$ m·s^{-1} et $U_j = 40$ m·s^{-1}. Pour $U_j = 20$ m·s^{-1}, la couche limite naturelle en sortie de buse est laminaire. En présence du forçage, les fluctuations du premier et du second sous-harmonique de la fréquence de l'excitation sont détectées dans la couche de cisaillement. Par ailleurs, le champ proche du premier sous-harmonique de la pression mesuré le long du jet est constitué de deux maxima de forme sinusoïdale. Le diagramme de directivité en champ lointain possède deux lobes séparés par un angle d'extinction $\theta^\star$ autour de 85° de l'axe du jet. Ces observations sont en accord avec les résultats de Bridges concernant le bruit d'appariement tourbillonnaire. En revanche, pour $U_j = 40$ m·s^{-1}, la couche limite initiale est transitionnelle et seul le premier sous-harmonique est observé lorsque l'excitation est utilisée. Dans ce cas, le champ de pression proche en périphérie du jet est de forme gaussienne et le champ acoustique lointain est superdirectif, comme observé par Laufer et Yen. L'état initial de la couche de cisaillement semble être le facteur déterminant pour distinguer ces deux rayonnements très différents. ***Pour citer cet article : V. Fleury et al., C. R. Mecanique 333 (2005).***

* Corresponding author.
E-mail addresses: vincent.fleury@ec-lyon.fr (V. Fleury), christophe.bailly@ec-lyon.fr (C. Bailly).
URL: http://acoustique.ec-lyon.fr.

1631-0721/$ – see front matter
doi:10.1016/j.crme.2005.09.003

Keywords: Fluid mechanics; Excited jet; Subharmonic; Pairing noise; Superdirective radiation

Mots-clés : Mécanique des fluides ; Jet excité ; Sous-harmonique ; Bruit d'appariement ; Rayonnement superdirectif

Version française abrégée

Dans son analyse du bruit produit par un jet subsonique excité, Kibens [1] a montré la possibilité de réduire les fluctuations du jet à quelques structures sous-harmoniques de la fréquence du forçage. Ce présent travail expérimental décrit le rayonnement acoustique du premier sous-harmonique. Deux types d'émissions acoustiques très différentes sont indiquées dans la littérature. Bridges [2] rend compte d'un champ lointain constitué de deux lobes de directivité séparés par un angle d'extinction $\theta^\star$ proche de 70° de l'axe aval du jet. Ce rayonnement est interprété comme résultant de l'appariement des structures de vorticité au centre de la couche de cisaillement. Le second type d'émission a été observé par Laufer et Yen [3] et est caractérisé par un rayonnement très intense vers l'aval. Ce diagramme d'émission dit superdirectif, est associé par Crighton et Huerre [4] à l'allure gaussienne du champ de pression sous-harmonique le long de la couche de cisaillement. Notre étude vise à caractériser et à distinguer les conditions de l'écoulement à l'origine de ces deux formes de rayonnement.

Nous disposons d'un jet de diamètre $D = 5$ cm en environnement anéchoïque. Deux vitesses de jet, $U_j = 20\ \mathrm{m{\cdot}s^{-1}}$ et $U_j = 40\ \mathrm{m{\cdot}s^{-1}}$ ont été considérées, correspondant à des nombres de Reynolds Re_D de $6{,}7 \times 10^4$ et $1{,}3 \times 10^5$ respectivement. En l'absence de forçage, la couche limite en sortie de buse est laminaire pour $U_j = 20\ \mathrm{m{\cdot}s^{-1}}$, voir la Fig. 1(a) et le Tableau 1. La couche de cisaillement initiale est excitée acoustiquement au moyen de quatre haut-parleurs disposés en périphérie de buse. La fréquence de l'excitation f_{ex} est voisine de la fréquence privilégiée f_0 de la couche de cisaillement naturelle, voir le Tableau 2. Pour $U_j = 20\ \mathrm{m{\cdot}s^{-1}}$, la fluctuation de vitesse au centre de la couche de cisaillement est constituée principalement du fondamental f_{ex}, du premier sous-harmonique $f_{\mathrm{s1}} = f_{\mathrm{ex}}/2$ et du second sous-harmonique $f_{\mathrm{s2}} = f_{\mathrm{ex}}/4$. Ces ondes d'instabilité croissent rapidement depuis la sortie de la buse et saturent respectivement en $x_{\mathrm{ex}} \approx 0.25D$, $x_{\mathrm{s1}} = 2x_{\mathrm{s0}}$ et $x_{\mathrm{s2}} = 4x_{\mathrm{s0}}$, voir la Fig. 2(a). Un transfert d'énergie s'opère alors en faveur des harmoniques. En particulier, le premier harmonique de la composante f_{s2}, soit $2 \times f_{\mathrm{s2}} = f_{\mathrm{s1}}$, est alimenté en x_{s2}, ce qui conduit à un second maximum du premier sous-harmonique f_{s1}. Pour $U_j = 40\ \mathrm{m{\cdot}s^{-1}}$, la couche limite en sortie de buse est transitionelle, voir la Fig. 1(a) et le Tableau 1 et aucun second sous-harmonique f_{s2} n'est décelé au centre de la couche de cisaillement. La composante f_{s1} de la vitesse fluctuante présente un unique maximum, voir la Fig. 2(b). Ces maxima des sous-harmoniques de la vitesse indiquent la présence d'appariements tourbillonnaires s'opérant de manière périodique au centre de la couche de cisaillement, voir [5]. Dans le cas de conditions initiales laminaires, $U_j = 20\ \mathrm{m{\cdot}s^{-1}}$, ce processus d'appariements successifs est stable [1]. En revanche, en présence de conditions transitionnelles, $U_j = 40\ \mathrm{m{\cdot}s^{-1}}$, les structures cohérentes de vorticité sont fortement perturbées par les fluctuations turbulentes et se détruisent lors du premier appariement en x_{s1}, voir [6]. Le second appariement est alors inhibé plus en aval, ce qui empêche la production du second sous-harmonique.

Le champ de pression proche a par ailleurs été mesuré le long de la couche de cisaillement, au voisinage de la saturation des sous-harmoniques de la vitesse. Pour $U_j = 20\ \mathrm{m{\cdot}s^{-1}}$, le champ du sous-harmonique f_{s1} de la pression présente 2 lobes de forme sinusoïdale, voir la Fig. 3(a) et l'expression (2). La directivité du champ acoustique lointain est également constituée de 2 lobes séparés par un angle d'extinction autour de 85°, voir la Fig 5(a). Ces observations sont en accord avec les résultats de Bridges [2]. Pour $U_j = 40\ \mathrm{m{\cdot}s^{-1}}$, le champ du sous-harmonique f_{s1} de la pression présente en revanche un unique maximum, voir la Fig. 3(a). Cette distribution du champ de pression proche est de forme gaussienne et le rayonnement acoustique est superdirectif, voir la Fig. 5(b). Ce résultat est conforme aux observations de Laufer et Yen [3]. Il semble que la présence ou non du second sous-harmonique f_{s2} de la fluctuation de vitesse au centre de la couche de cisaillement distingue ces deux formes d'émission acoustique.

1. Introduction

For a perfectly expanded supersonic jet, Mach waves are the dominant noise component and are associated to the radiation of instability waves whose phase speed is supersonic relative to the ambient medium, see Tam and Burton [7] or Tam [8] for a review. It is very attractive to extend this aeroacoustic mechanism to subsonic jets. Recent studies have shown that the radiation of a subsonic jet in the downstream direction is directly linked to the dynamics of

coherent structures at the end of the potential core, and that the directivity pattern is quite similar to the radiation of instability waves [9,10]. However in such a flow, any convective instability wave travels with a subsonic phase speed and is thus not expected to produce intense far-field noise. This paradox may be solved by considering the spatial evolution of the instability wave along a large region of the spreading jet flow. As shown by Crighton and Huerre [4], the envelope may be spatially wide enough to hold large-scale supersonic components which can then contribute to the far-field noise. This interpretation gives a new insight of the subsonic jet noise mechanisms.

In the present work, the acoustic radiation by instability waves in the shear-layer of a low-Mach-number jet is investigated experimentally. An external acoustic tone excitation at a frequency close to the most-unstable frequency of the natural shear-layer is applied to organize artificially the fluctuations. Discrete subharmonic fluctuations are then observed as in Kibens [1] and the acoustic radiation by the first subharmonic is especially focused on. Two different directivity patterns mentioned in the literature are to be distinguished, namely the so-called superdirective radiation and the vortex pairing noise. The superdirective radiation has been observed experimentally by Laufer and Yen [3] and is characterized by a very sharp beaming in the downstream direction. This pattern would result from the Gaussian shape of the slowly spatially modulated subharmonic pressure field along the spreading shear-layer as argued by Crighton and Huerre [4]. The acoustic emission by vortex pairing in a jet has been reported first by Bridges [2]. The directivity shows two lobes separated by an extinction angle and is attributed to the quadrupolar noise radiation by vorticity in the annular shear-layer, as discussed by Möhring [11], for instance. The experimental conditions and the noise mechanisms leading to each of these acoustic fields have been partially documented. In the present study, these two radiation patterns have been observed in the same facility and some flow and acoustic measurements are reported. The conditions of the initial shear-layer are found discriminant.

2. Experimental facility and natural flow characteristics

The experiments were conducted in one of the anechoic chambers of the École centrale de Lyon (6.10 m × 4.60 m × 3.80 m). A thorough characterization of the facility can be found in Berhault et al. [12]. The jet diameter is $D = 5$ cm and two velocities are considered, $U_j = 20$ m·s^{-1} and $U_j = 40$ m·s^{-1}. The Reynolds numbers based on D are thus $Re_D = 6.7 \times 10^4$ and 1.3×10^5, respectively. The flow is powered by an upstream fan and conditioned by mufflers, screens and honeycombs. In addition, the jet nozzle applies a contraction by the section ratio of 46/1.

The excitation device consists of four loudspeakers with independent but identical acoustic cavities. The disturbance is generated at $\theta = 110°$ to the flow direction through a 2 mm wide circular slot opening at the nozzle exit. It can be considered axisymmetric as the phase of the acoustic perturbation shifts of less than 20° from one cavity exit to the other.

Velocity measurements were performed using a 5 μm diameter and 1.25 mm long tungsten-wire mounted on a Dantec Streamline constant temperature anemometer. The overheat ratio was 0.80 and the frequency response was optimized up to 20 kHz, which is sufficient in this work. The near pressure field was measured with a $1/8''$ B&K microphone and the acoustic far-field with a $1/2''$ B&K microphone. Power spectra density were carried out by a HP 35652B analyser and the frequency resolution was taken to be 8 Hz. Between 1000 and 2000 spectra were acquired to calculate the velocity and pressure spectra, denoted by u'_f and p'_f, respectively. Root-mean-square fluctuating velocity data, u', were measured by a multimeter in the frequency range 20 Hz – 20 kHz. Around 500 data were required to get statistics convergence.

The turbulence intensity in the potential core, at the nozzle exit, u'_{pc}/U_j compares well with the usual 0.3% value mentioned in the literature for natural (not excited) jets, see Table 1. The boundary-layer profile of the natural jets was investigated at $x = 0.5$ mm downstream the nozzle exit and is given in Fig. 1(a). The mean velocity profiles for the two velocities are in good agreement with the Blasius profile. However, the turbulence intensity increases strongly as U_j varies from 20 to 40 m·s^{-1}. This trend was also observed by Zaman [13] and Hussain [9], and is attributed to a Reynolds number effect. Following Zaman's classification, the boundary-layer is laminar when Re_D is below 10^5, and nominally laminar above, namely for $U_j = 20$ m·s^{-1} and $U_j = 40$ m·s^{-1}, respectively, in our case.

The shear-layer of the natural jets was investigated at $x = 3.5$ mm and the mean velocity profiles are shown in Fig. 1(b). When $U_j = 40$ m·s^{-1}, the radial evolution of the mean velocity is well approximated by an hyperbolic tangent profile, whereas for $U_j = 20$ m·s^{-1}, a Blasius profile is in better agreement inside the jet. This indicates an incomplete transition of the boundary layer in the nozzle to the fully developed free shear-layer flow. In both cases, the

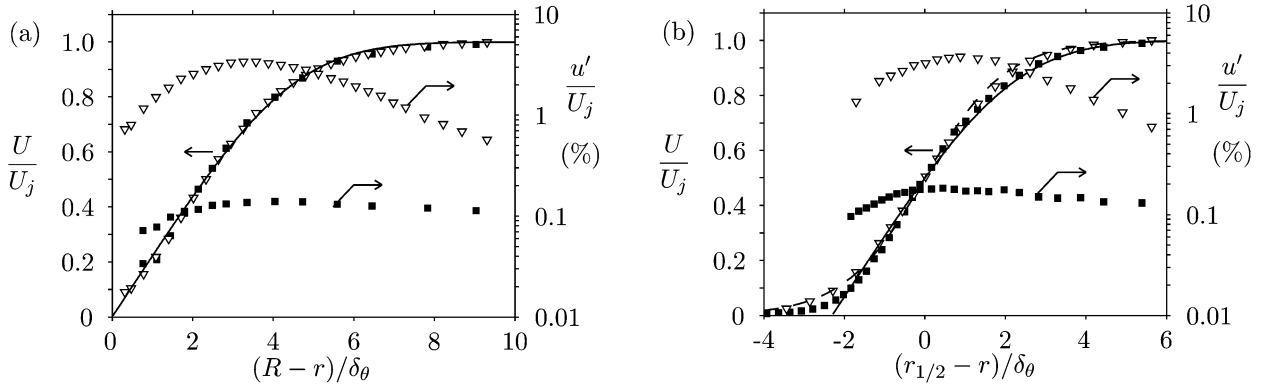

Fig. 1. Radial profiles of the mean and fluctuating axial velocities for the natural (unexcited) jet, ■ $U_j = 20$ m·s^{-1}; ▽ $U_j = 40$ m·s^{-1}: (a) boundary-layer profiles at $x = 0.5$ mm; (b) shear-layer profiles at $x = 3.5$ mm. r is the radial coordinate, $r = r_{1/2}$ is such that $U(r_{1/2}) = U_j/2$ and δ_θ is the momentum thickness. — Blasius profile; - - - hyperbolic tangent profile $U/U_j = 0.5[1 + \tanh(\eta)]$.

Fig. 1. Profils radiaux des vitesses axiales moyenne et fluctuante pour le jet naturel (non excité), ■ $U_j = 20$ m·s^{-1} ; ▽ $U_j = 40$ m·s^{-1} : (a) profils de la couche limite en $x = 0{,}5$ mm ; (b) profils de la couche de cisaillement en $x = 3{,}5$ mm. r est la coordonées radiale, $r = r_{1/2}$ est tel que $U(r_{1/2}) = U_j/2$ et δ_θ est l'épaisseur de quantité de mouvement. — profil de Blasius ; - - - profil en tangente hyperbolique $U/U_j = 0{,}5[1+\tanh(\eta)]$.

Table 1
Unexcited boundary-layer characteristics at the nozzle exit: $u'_{\rm bl}$ is the maximum fluctuating velocity in the boundary-layer, $u'_{\rm pc}$ is the fluctuating velocity in the potential core center for $x = 0$, Re_{δ_θ} is the momentum thickness Reynolds number, δ_1 is the displacement thickness and H is the shape factor

Tableau 1
Caractéristiques de la couche limite naturelle en sortie de buse : $u'_{\rm bl}$ est la vitesse fluctuante maximale dans la couche limite, $u'_{\rm pc}$ est la fluctuation de vitesse au centre du cône potentiel pour $x = 0$, Re_{δ_θ} est le nombre de Reynolds de la couche limite, δ_1 est l'épaisseur de déplacement et H est le facteur de forme

U_j (m·s^{-1})	Re_D	$u'_{\rm bl}/U_j$ %	$u'_{\rm pc}/U_j$ %	δ_θ/D	Re_{δ_θ}	$H = \delta_1/\delta_\theta$
20	6.7×10^4	0.14	0.10	0.0023	160	2.56
40	1.3×10^5	3.34	0.36	0.0026	373	2.56

Table 2
Characteristics of the natural shear-layer at $x \approx 3.5$ mm and of the excitation. $u'_{\rm sl}$ is the maximum turbulent velocity in the unexcited shear-layer

Tableau 2
Caractéristiques de la couche de cisaillement naturelle à $x \approx 3{,}5$ mm et de l'excitation. $u'_{\rm sl}$ est la vitesse turbulente maximale dans la couche de cisaillement non excitée

U_j (m·s^{-1})	$u'_{\rm sl}/U_j$	δ_θ/D	f_0 (Hz)	$St_{\delta_\theta}(f_0)$	$f_{\rm ex}$ (Hz)	$u'_{f_{\rm ex}}(x \approx 0)/U_j$	$u'_{f_{\rm ex}}(x_{\rm s1})/U_j$
20	0.18%	0.0042	1300	0.0137	1500	0.05%	7.5%
40	3.66%	0.0028	4100	0.0144	3530	0.10%	11%

maximum turbulence intensity has not increased strongly from $x = 0.5$ mm to $x = 3.5$ mm. These flow characteristics are given in Table 2.

3. Spectral analysis of the excited shear-layer

The velocity spectra recorded in the initial shear-layer of the natural jet display a typical tone fluctuation whose frequency f_0 corresponds to the most amplified instability wave of the local sheared flow as shown by Michalke [14] and confirmed experimentally by Freymuth [15]. The associated Strouhal number $St_{\delta_\theta} = f_0\delta_\theta/U_j$ is found close to the theoretical value 0.017, valid for small values of δ_θ/D, see Table 2. Following Kibens [1], the acoustic excitation frequency $f_{\rm ex}$ is taken close to f_0 in order to drive efficiently the fluctuations in the shear-layer. In the initial region, these fluctuations are then mostly constituted of a few subharmonics of $f_{\rm ex}$. The level of the excitation is characterized,

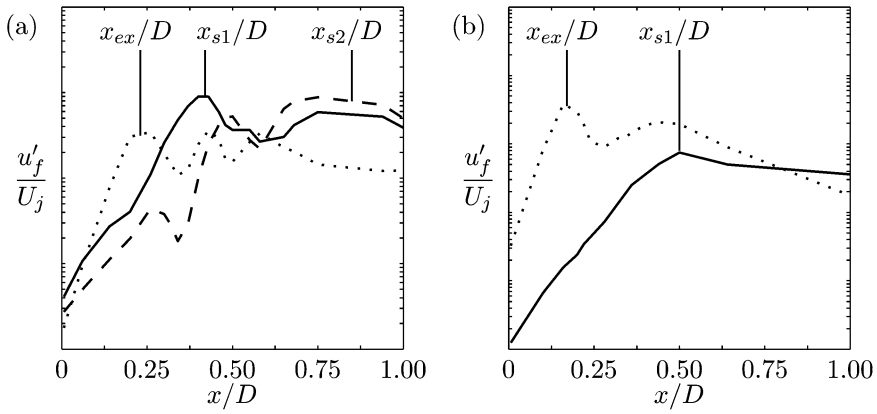

Fig. 2. Axial evolution of the fundamental and subharmonics of the fluctuating velocity in the center of the shear-layer $r = D/2$. The total turbulence intensity is displayed as well. (a) $U_j = 20$ m·s^{-1}; (b) $U_j = 40$ m·s^{-1}. $\cdots\ u'_{f_{ex}}/U_j^2$; — $u'_{f_{s1}}/U_j^2$; - - - $u'_{f_{s2}}/U_j^2$; ··· u'/U_j.

Fig. 2. Évolution axiale du fondamental et des sous-harmoniques de la vitesse fluctuante au centre de la couche de cisaillement $r = D/2$. Le niveau de turbulence total est également montré. (a) $U_j = 20$ m·s^{-1} ; (b) $U_j = 40$ m·s^{-1}. $\cdots\ u'_{f_{ex}}/U_j^2$; — $u'_{f_{s1}}/U_j$; - - - $u'_{f_{s2}}/U_j$; ··· u'/U_j.

either by the fluctuation rate in the center of the initial shear-layer $u'_{f_{ex}}(x \approx 0)/U_j$, or by the maximum rate $u'_{f_{ex}}(x = x_{ex})/U_j$ along the shear-layer, see Table 2. For a comparison, Laufer and Yen [3] found for $u'_{f_{ex}}(x_{ex})/U_j$ between 2 and 7.6%.

For $U_j = 20$ m·s^{-1}, Fig. 2(a) shows the axial evolution of $u'_{f_{ex}}$, $u'_{f_{s1}}$ and $u'_{f_{s2}}$ along the shear-layer at $r = D/2$. The frequencies $f_{s1} = f_{ex}/2$ and $f_{s2} = f_{ex}/4$ correspond to the first and second subharmonics, respectively. After a very fast growth from the nozzle exit, these components saturate in $x_{ex} \approx 0.25D$, $x_{s1} \approx 2x_{ex}$ and $x_{s2} \approx 4x_{ex}$, respectively. At these locations, energy is transferred to higher harmonics as observed in x_{s2} for instance, where energy is supplied to the harmonic $2 \times f_{s2} = f_{s1}$ and produces a second maximum for $u'_{f_{s1}}$. The presence of the maxima of $u'_{f_{s1}}$ and $u'_{f_{s2}}$ indicates the occurrence of two successive vortex pairing stages and shows the stable evolution of the pairing cascade [1].

For $U_j = 40$ m·s^{-1}, the second subharmonic $u'_{f_{s2}}$ is not observed in the turbulent velocity spectra performed in the shear-layer. The second pairing stage is indeed inhibited in this configuration. This is due to the breakdown of coherent ring vortex structures during the first pairing, caused by strong random perturbations in the transitional shear-layer. The axial evolution of $u'_{f_{s1}}$ plotted in Fig. 2(b) is thus different from the laminar jet configuration at $U_j = 20$ m·s^{-1}, and presents only one saturation.

4. Subharmonic near pressure field

The near pressure field was measured in the close vicinity of the jet, at around $D/5$ from the center of the shear-layer. The microphone was traveled in the axial direction following a direction θ of 10°, in order to take into account the slow divergence of the jet. Only the first subharmonic component of the pressure, $p'_{f_{s1}} = E(x) \times e^{i\phi(x)}$, is concerned here.

For $U_j = 40$ m·s^{-1}, the x dependence of the envelope $E(x)$ is displayed in Fig. 3(a). As noticed by Laufer and Yen [3], it can be represented by a Gaussian:

$$E(x) \propto \exp\left\{-\left(\frac{x - x_{s1}}{\sigma_e}\right)^2\right\} \tag{1}$$

where x_{s1} is the location of the pressure maximum and σ_e the length-scale of the envelope. For $U_j = 20$ m·s^{-1}, the evolution of $E(x)$ is quite different, as shown in Fig. 3(a). Two strong maxima are observed for axial positions close to the saturations of $u'_{f_{s1}}$ in the shear-layer center [16]. A model distribution constituted of two sinusoidal arches is proposed for describing the axial evolution of $E(x)$:

$$E(x) = \cos\left(\pi \frac{x - x_{s1}}{\sigma_e}\right) B(x, x_{s1}, \sigma_e) + P_{21} \cos\left(\pi \frac{x - x_{s2}}{\sigma_e}\right) B(x, x_{s2}, \sigma_e) \tag{2}$$

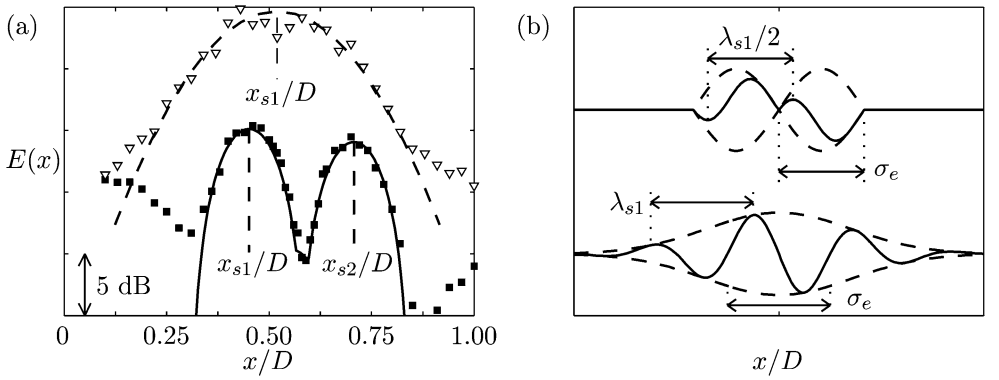

Fig. 3. Near pressure field of $|p_{f_{s1}}|$ along the spreading jet: (a) experimental data. ■ $U_j = 20$ m·s^{-1}; ▽ $U_j = 40$ m·s^{-1}; - - - Gaussian model (1); — sinusoidal model (2); (b) sketch of the pressure field. Aspect ratios σ_e/λ_{s1} and λ_e/λ_{s1} are preserved. — fluctuating pressure; - - - envelope of the pressure field.

Fig. 3. Pression en champ proche de $|p_{f_{s1}}|$ le long du jet : (a) mesures. ■ $U_j = 20$ m·s^{-1} ; ▽ $U_j = 40$ m·s^{-1} ; - - - modèle gaussien (1) ; — modèle sinusoïdal (2) ; (b) schéma du champ de pression. Les rapports d'échelles σ_e/λ_{s1} et λ_e/λ_{s1} sont préservés. — pression fluctuante ; - - - enveloppe du champ de pression.

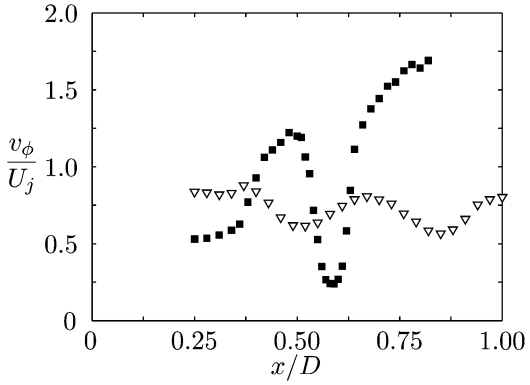

Fig. 4. Phase speed v_ϕ of $p_{f_{s1}}$: ■ $U_j = 20$ m·s^{-1}; ▽ $U_j = 40$ m·s^{-1}.

Fig. 4. Vitesse de phase v_ϕ de $p_{f_{s1}}$: ■ $U_j = 20$ m·s^{-1} ; ▽ $U_j = 40$ m·s^{-1}.

where $B(x, x_{si}, \sigma_e)$ is the boxcar function, equal to one for $|x - x_{si}| < \sigma_e/2$ and zero otherwise. The parameter P_{21} ($= 0.957$) is the pressure ratio between x_{s2} and x_{x1}, and the envelope characteristic length-scale σ_e is chosen as the size of one sinusoidal arch.

The spatial evolution of the phase $\phi(x)$ has been measured by taking a reference microphone located in the near pressure field, at $x = D/2$ and at 90° azimuthally from the traveling microphone. The phase speed v_ϕ is then obtained by derivation, $v_\phi(x) = 2\pi f_{s1}/(\mathrm{d}\phi/\mathrm{d}x)$, and the result is reported in Fig. 4. This velocity is far from constant and may be higher than typical values found for pure aerodynamic fluctuations, usually around $0.6U_j$. Note that both the aerodynamic and the acoustic contributions exist in the near pressure field.

The knowledge of the phase velocity allows us to estimate a mean value of the wavelength $\lambda_{s1} = v_\phi/f_{s1}$ of the pressure wave $p'_{f_{s1}}$. For the Gaussian envelope (1) at $U_j = 40$ m·s^{-1}, λ_{s1} is estimated by using the phase speed at the maximum $x = x_{s1}$. For $U_j = 20$ m·s^{-1}, $\lambda_{s1}/2$ is approximated by the distance between the two pressure lobes $|x_{s2} - x_{s1}|$, which yields a phase speed of $0.9U_j$.

All the scales involved above are given in Table 3. A sketch is also shown in Fig. 3(b) for both the Gaussian and sinusoidal configurations. Note that the pressure field is acoustically compact in the two cases since the acoustic wavelength $\lambda_{ac} = c_\infty/f_{s1}$ is far larger than the radial D and the axial scale σ_e, c_∞ being the sound speed outside the jet.

Table 3
Characteristics of the near pressure field. $M_p = v_\phi/c_\infty = f_{s1}\lambda_{s1}/c_\infty = \lambda_{s1}/\lambda_{ac}$ is the phase Mach number

Tableau 3
Caractéristiques du champ de pression proche. $M_p = v_\phi/c_\infty = f_{s1}\lambda_{s1}/c_\infty = \lambda_{s1}/\lambda_{ac}$ est le nombre de Mach de la phase

U_j (m·s^{-1})	σ_e/D	λ_{s1}/D	λ_{ac}/D	σ_e/λ_{s1}	λ_{ac}/σ_e	M_p
20	0.3	0.5	9.1	0.6	30.4	$0.9M_j$
40	0.3	0.3	3.8	1.0	12.8	$0.7M_j$

5. Subharmonic far pressure field

The acoustic directivity of $p'_{f_{s1}}$ is shown in Fig. 5(a) for $U_j = 20$ m·s^{-1}. The measurement was performed at $40D$ from the nozzle exit for different angular positions θ to the jet axis. This pattern is in good agreement with the experimental data of Bridges [2], usually referred to as vortex pairing noise. A typical extinction angle is observed for $\theta^\star$ around 85°. For $U_j = 40$ m·s^{-1}, the directivity pattern is quite different, see Fig. 5(b), and the acoustic radiation takes place mainly in the downstream direction. The range is also much higher, around 25 dB with respect to about 15 dB for $U_j = 20$ m·s^{-1}. This emission collapses fairly well with the superdirective distribution given by Laufer and Yen [3] for $M_p \ll 1$:

$$|p'_{f_{s1}}| \propto \exp\{45 \times M_p \cos\theta\} \tag{3}$$

The transition between the near pressure field and the acoustic far field is displayed in Figs. 6(a) and 6(b), where d stands for the distance to the point ($x = D/2$, $r = D/2$). Two directions $\theta = 90°$ and $\theta = 20°$ are considered. The results show an exponential decay close to the jet with more than 40 dB attenuation for the two velocities U_j and the two θ directions.

The near pressure field $p'_{f_{s1}}$ varies according to the radial distance to the center of the shear-layer $|r - D/2| = d\sin\theta$ and the attenuation rate is of the order of the wave-number $k_{s1} = 2\pi/\lambda_{s1}$:

$$|p_{f_{s1}}| \propto \exp\{-\alpha k_{s1} d \sin\theta\} \tag{4}$$

where $\alpha > 0$ is a parameter. For $U_j = 40$ m·s^{-1}, $\alpha \simeq 2$ in the two directions. For $U_j = 20$ m·s^{-1}, the initial decay is faster and the values of α differ with θ, $\alpha \approx 3$ for $\theta = 90°$ and $\alpha \approx 4$ for $\theta = 20°$. As d increases, the classical $1/d$ decay law is recovered, as reported in Fig. 6(b).

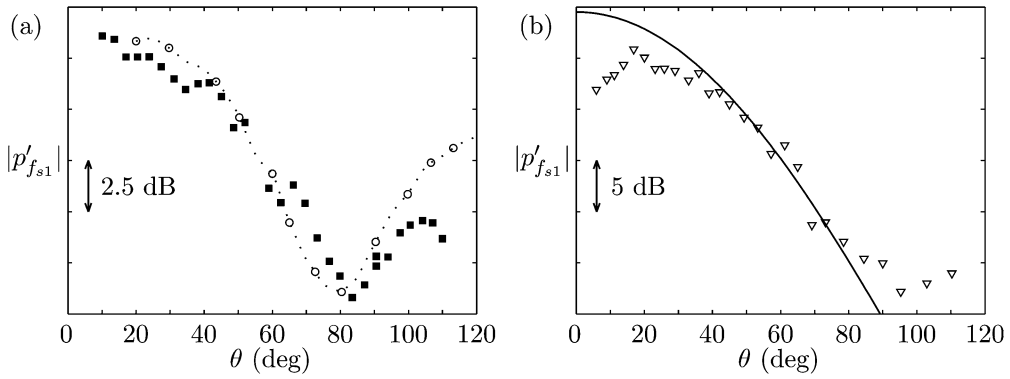

Fig. 5. Acoustic directivity of $p_{f_{s1}}$: (a) ■ $U_j = 20$ m·s^{-1}; · ○ · Bridges [2] (Fig. 2.7, doubly stable pairing, component $f_{ex}/2$). (b) ▽ $U_j = 40$ m·s^{-1}; — superdirective pattern (3).

Fig. 5. Directivité acoustique de $p_{f_{s1}}$: (a) ■ $U_j = 20$ m·s^{-1} ; · ○ · Bridges [2] (Fig. 2.7, appariement doublement stable, composante $f_{ex}/2$). (b) ▽ $U_j = 40$ m·s^{-1} ; — rayonnement superdirectif (3).

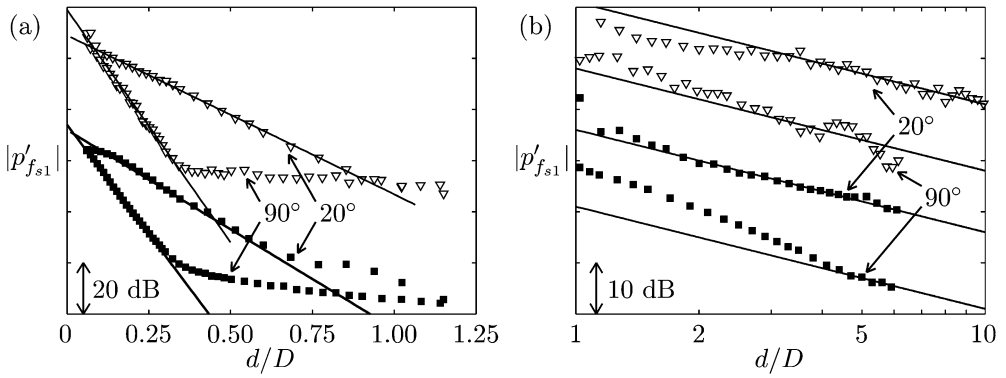

Fig. 6. Decay of $|p_{f_{s1}}|$ along two directions $\theta = 20°$ and $\theta = 90°$. ■ $U_j = 20$ m·s^{-1}; ▽ $U_j = 40$ m·s^{-1}. (a) — exponential expression (4); (b) — $1/d$ law.

Fig. 6. Décroissance de $|p_{f_{s1}}|$ selon deux directions $\theta = 20°$ et $\theta = 90°$. ■ $U_j = 20$ m·s^{-1} ; ▽ $U_j = 40$ m·s^{-1}. (a) — expression exponentielle (4) ; (b) — loi en $1/d$.

6. Conclusion

Two different patterns of subharmonic radiation by an excited shear-layer were observed. For $U_j = 20$ m·s^{-1}, a two-lobe directivity with a typical extinction angle was measured, in good agreement with the vortex pairing noise found by Bridges [2]. For $U_j = 40$ m·s^{-1}, the radiation diagram is monotonic and highly directive downstream as observed by Laufer and Yen [3]. The distinction is attributed to the shape of the near pressure field $p'_{f_{s1}}$ along the shear-layer, directly linked to the presence or not of the second subharmonic of the fluctuating velocity. Moreover an exponential decay of the pressure field is measured near the jet before reaching the classical $1/d$ decay. In a companion paper [17], the experimental models (1) and (2) for the near pressure field are used to predict the two different patterns of subharmonic radiated acoustic field.

Acknowledgement

The authors are grateful to Professor Geneviève Comte-Bellot for her helpful comments during this work.

References

[1] V. Kibens, Discrete noise spectrum generated by an acoustically excited jet, AIAA J. 18 (4) (1980) 434–441.
[2] J.E. Bridges, Application of coherent structure and vortex sound theories to jet noise, Ph.D. Dissertation, University of Houston, 1990.
[3] J. Laufer, T.-C. Yen, Noise generation by a low-Mach-number jet, J. Fluid Mech. 134 (1983) 1–31.
[4] D.G. Crighton, P. Huerre, Shear-layer fluctuating pressure and superdirective acoustic sources, J. Fluid Mech. 220 (1990) 355–368.
[5] C.-M. Ho, L.-S. Huang, Subharmonics and vortex merging in mixing layers, J. Fluid Mech. 119 (1982) 443–473.
[6] A.K.M.F. Hussain, K.B.M. Zaman, Vortex pairing in a circular jet under controlled excitation. Part 2. Coherent structure dynamics, J. Fluid Mech. 101 (1980) 493–544.
[7] C.K.W. Tam, D.E. Burton, Sound generated by instability waves of supersonic flows. Part 2, axisymmetric jets, J. Fluid Mech. 138 (1984) 273–295.
[8] C.K.W. Tam, Supersonic jet noise, Annu. Rev. Fluid Mech. 27 (1995) 17–43.
[9] A.K.M.F. Hussain, Coherent structures and turbulence, J. Fluid Mech. 173 (1986) 303–356.
[10] C. Bogey, C. Bailly, D. Juvé, Noise investigation of a high subsonic, moderate Reynolds number jet using a compressible LES, Theoret. Comput. Fluid Dynam. 16 (4) (2003) 273–297.
[11] W. Möhring, On vortex sound at low Mach number, J. Fluid Mech. 85 (1978) 685–691.
[12] J.M. Berhault, M. Sunyach, H. Arbey, G. Comte-Bellot, Réalisation d'une chambre anéchoïque revêtue de panneaux et destinée à l'étude des bruits d'origine aérodynamique, Acustica 29 (2) (1973) 69–78.
[13] K.B.M.Q. Zaman, Far-field noise of a subsonic jet under controlled excitation, J. Fluid Mech. 152 (1985) 83–111.
[14] A. Michalke, On spatially growing disturbances in an inviscid shear layer, J. Fluid Mech. 23 (1965) 521–544.
[15] P. Freymuth, On the transition in a separated laminar boundary layer, J. Fluid Mech. 25 (1966) 683–704.
[16] J.E. Bridges, F. Hussain, Direct evaluation of aeroacoustic theory in a jet, J. Fluid Mech. 240 (1992) 469–501.
[17] V. Fleury, C. Bailly, D. Juvé, Shear-layer acoustic radiation in an excited subsonic jet: Models for vortex pairing and superdirective noise, C. R. Mecanique 333 (2005), in this issue.